

# CHAPTER 4

## 1:6-Scale Frame: Stiffness and Modal Testing

### 4.1 OVERVIEW

A 1:6-scale steel moment frame was designed for shaking-table experiments described in Chapter 5 based on Drain-2DX (DRAIN) analyses. Three frames were fabricated for the 1:6-scale shaking table experiments using typical steel fabrication practices. Two frames were used in experiments and are referred to herein as Frame 1 and Frame 2. Frame 1 denotes the moment frame tested without ropes and Frame 2 denotes the moment frame tested with ropes during the Northridge ground-motion testing described in Chapter 5. The third frame was held in reserve to be used only if a problem invalidating test results of Frame 1 or Frame 2 was encountered. No such problems occurred. It should be noted that ropes were not installed in Frame 2 for the static and modal testing described in this Chapter.

The DRAIN model development and analyses, resulting in the proportioning of standard hollow structural steel (HSS) sections for the 1:6-scale frame, is presented in detail in Chapter 3. For the DRAIN analyses, several frame properties impacting frame stiffness and damping were based on state-of-practice principles. Although these principles are widely regarded as acceptable and safe in practice, a satisfactory estimate of the response of the frame when subjected to shaking table accelerations required the actual stiffness, resonant modes, and damping of the frame. Three types of experimental tests were used to determine these properties: stiffness tests, impact hammer tests, and low-amplitude, sinusoidal base-input tests. The DRAIN model was modified based on the findings of these tests.

When planning the shaking table experiments, both frames were assumed to be identical. However, fabricating two perfectly identical frames was not practically possible, particularly in light of typical steel fabrication practices used to construct the frames. Although great care was taken to ensure quality of fabrication, some minor differences between Frame 1 and Frame 2 were expected. This was determined to be acceptable, provided that the differences between the frames could be identified and subsequently determined to have little or no impact on the outcome of the shaking table tests. To quantify the differences between the frames, stiffness tests, impact hammer tests, and low-amplitude sinusoidal base input tests were conducted.

This chapter describes the fabrication and fit-up practices used to construct the 1:6-scale model frames and the aspects of the frame that were difficult to quantify analytically prior to fabricating the frame. The possible impact that fabrication and fit-up practices had on the variability between the responses of Frame 1 and Frame 2 is also discussed. Three experimental methods used to determine the actual stiffness, damping, and resonant modes of the frames are described, along with corresponding modifications to the analytical DRAIN model based on the modal and stiffness testing of Frame 1. Finally, the results of modal and stiffness tests conducted on Frame 2 are presented and compared to those of Frame 1. The overall goal of these tests was to improve the accuracy of the DRAIN model in predicting the 1:6-scale frame response when subjected to factored Northridge ground-motion input, and to quantify the differences between Frame 1 and Frame 2 with respect to dynamic and quasi-static lateral response.

## **4.2 DESCRIPTION OF EXPERIMENTAL FRAMES**

The experimental frames consisted of two primary components: a planar steel moment frame (Figure 4.1), and a four-column, auxiliary steel frame (leaner frame) (Figure 4.2). The purpose of the leaner frame was to support the floor and roof load vertically, while adding no lateral resistance to inertial loads. Two moment frames were used for testing, while one leaner frame was fabricated and used throughout the testing of both frames. An elevation and plan at the base of the test configuration are shown in Figure 4.3. All frames were fabricated at Irongate, Inc., located in Winchester, VA. Frame fit-up was initially conducted at Irongate using a mock-up of the Virginia Tech shaking table base plate (Figure 4.4). Components were subsequently disassembled and transported to Virginia Tech.

Each moment frame was installed on the shaking table one time. In other words, Frame 1 was installed, subjected to modal and stiffness testing described herein, subjected to Northridge ground-motion testing described in Chapter 5, and removed. Frame 2 was then installed on the shaking table with the leaner frame and subjected to modal and stiffness tests. Ropes were then added and Northridge ground-motion tests were conducted.

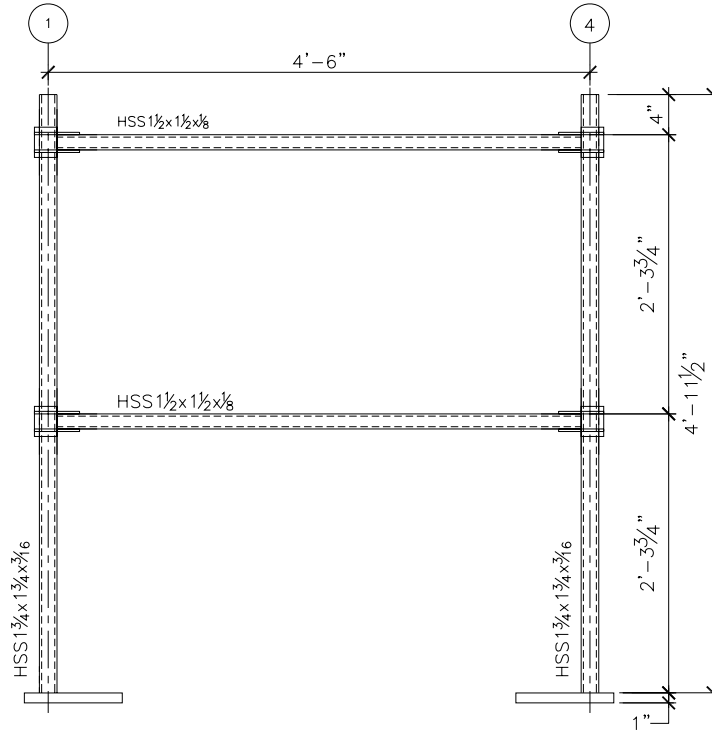


Figure 4. 1: Experimental Moment Frame

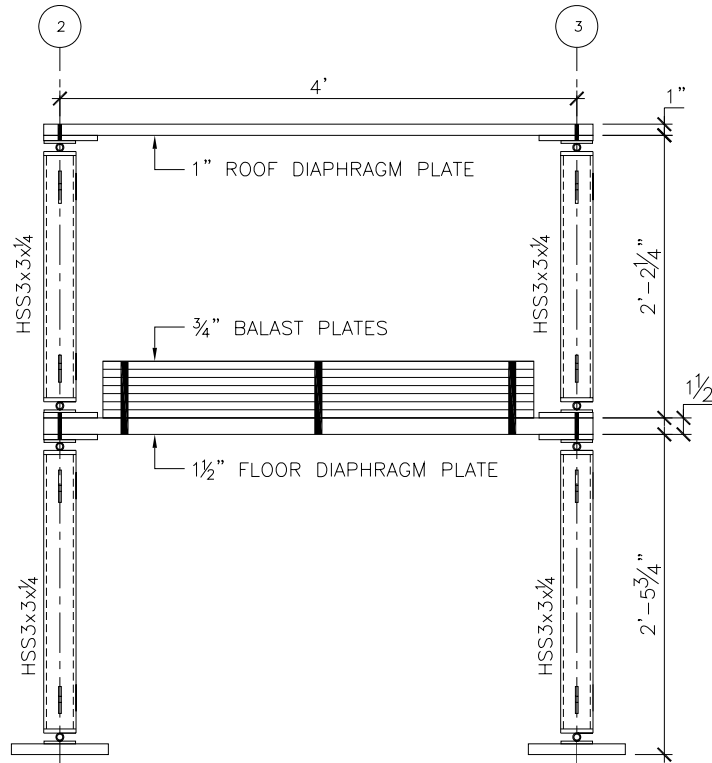


Figure 4. 2: Leaner Frame

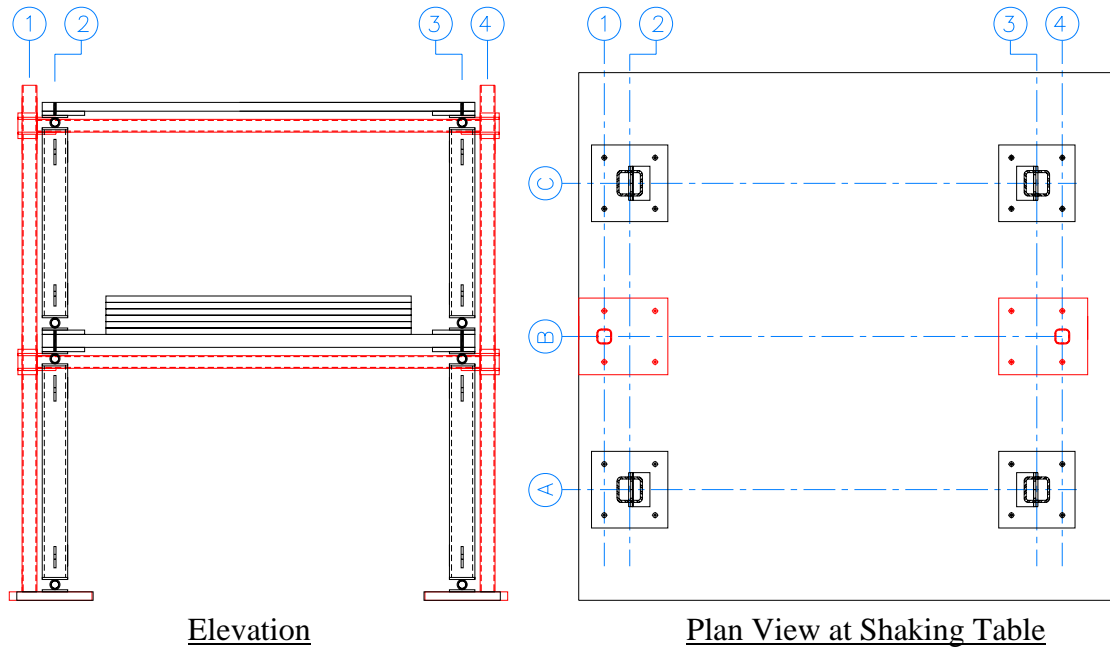


Figure 4. 3: Moment Frame and Leaner Frame in Testing Configuration



Figure 4. 4: Photograph of Mock-Up of Shaking Table Base Plate for Fit-Up at Irongate, Inc.

#### 4.2.1 PLANAR MOMENT FRAME

The steel moment frames consisted of HSS 1-3/4x1-3/4x3/16-A500 columns and HSS 1-1/2x1-1/2x1/8-A500 beams connected rigidly at the joints (Figure 4.5). Columns were rigidly attached to base plates, which were fastened to the shaking table with fully tensioned anchor bolts using the turn-of-the-nut method (AISC, 2005a) (Figure 4.6). See Appendix E for engineering drawings of the 1:6-scale frame.

As noted above, three moment frames were fabricated: one tested without ropes (Frame 1), one tested with ropes (Frame 2), and one to be held in reserve. Care was taken to minimize variability between frames during fabrication. To ensure material similarity, steel used for individual components was taken from the same heat of steel for all frames. To ensure geometric similarity, the moment frames were laid-out and welded in a jig. This process resulted in frames that visually appeared to be identical (Figure 4.7).



Figure 4. 6: Photograph of Connection at Beam-to-Column Joint



Figure 4. 5: Photograph of Connection at Column Base

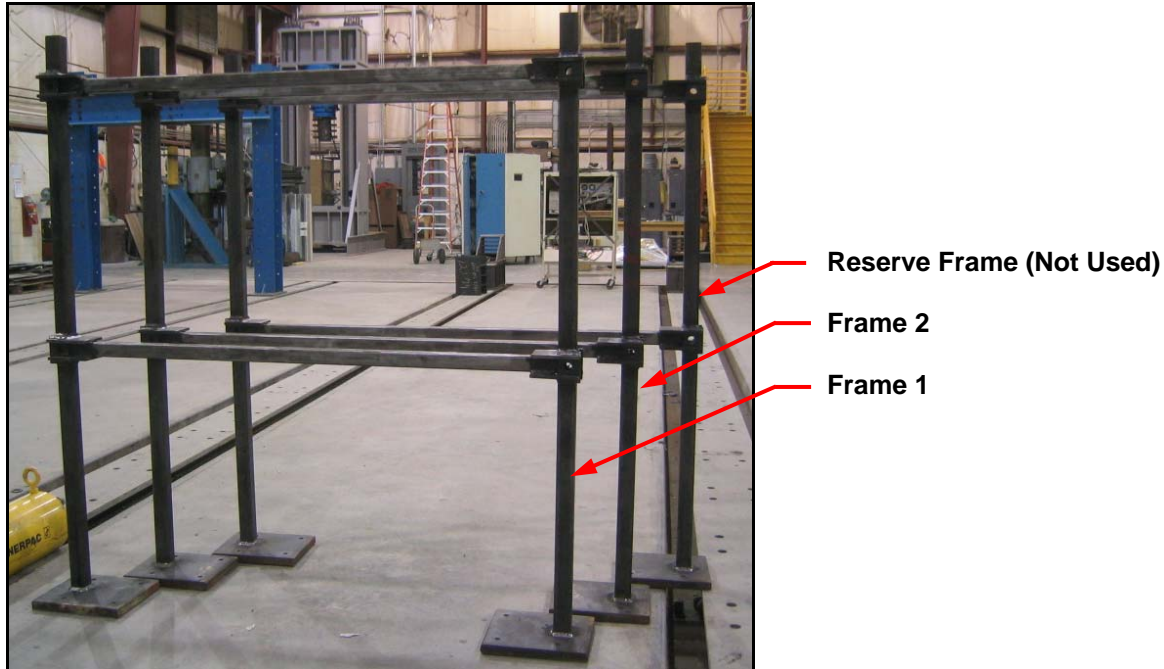


Figure 4. 7: Photograph of Moment Frames

Despite good quality control during fabrication, some aspects of the experimental frames varied slightly beyond the control of proper design and fabrication, causing inconsistencies between the idealized DRAIN model developed in Chapter 3 and the actual frame. Specifically, aspects that impacted the lateral stiffness of the moment frames included the wall thickness and overall dimensions of the HSS sections within mill tolerance, panel-zone stiffness, and the contribution of beam-to-column moment connections to the bending and shear flexibility of the beams and columns. The contribution to the lateral stiffness by these properties was investigated and the analytical DRAIN model was adjusted according to the findings, as reported in Section 4.3.

#### 4.2.2 LEANER FRAME

The leaner frame was a single-bay, 2-story frame. Steel plates were used for the roof and floor diaphragms and for additional floor ballast (Figure 4.8). The first-floor diaphragm was composed of a 1-1/2 in. x 4 ft 3 in. x 4 ft 6 in., A36, steel plate. Two stacks of seven, 3/4-in. x 1 ft 2 in. x 3 ft 4 in., A36, steel plates were used to complete the floor mass required. The roof diaphragm was composed of a 1 in. x 4 ft 3 in. x 4 ft 6 in., A36, steel plate. The floor and roof diaphragms were supported vertically by HSS 3 x 3 x 1/4-A500 columns. Each column was fabricated with hinges at the top and bottom, creating a rotational degree of freedom about a line

perpendicular to the line of the shaking-table motion. The hinges were fabricated with a 1-in.-diameter steel rod, seated in a round steel tube with a 1.125-in. inside diameter. Oil-impregnated brass bushings were machined to seat the rods in the round tube tightly, while providing minimal frictional resistance to rotation. In addition, bracing was added to the leaner frame perpendicular to the direction of shaking (Figure 4.9). This bracing was provided to prevent any torsional response at the roof and floor diaphragm relative to the shaking table. Engineering drawings of the leaner frame are shown in Appendix E.

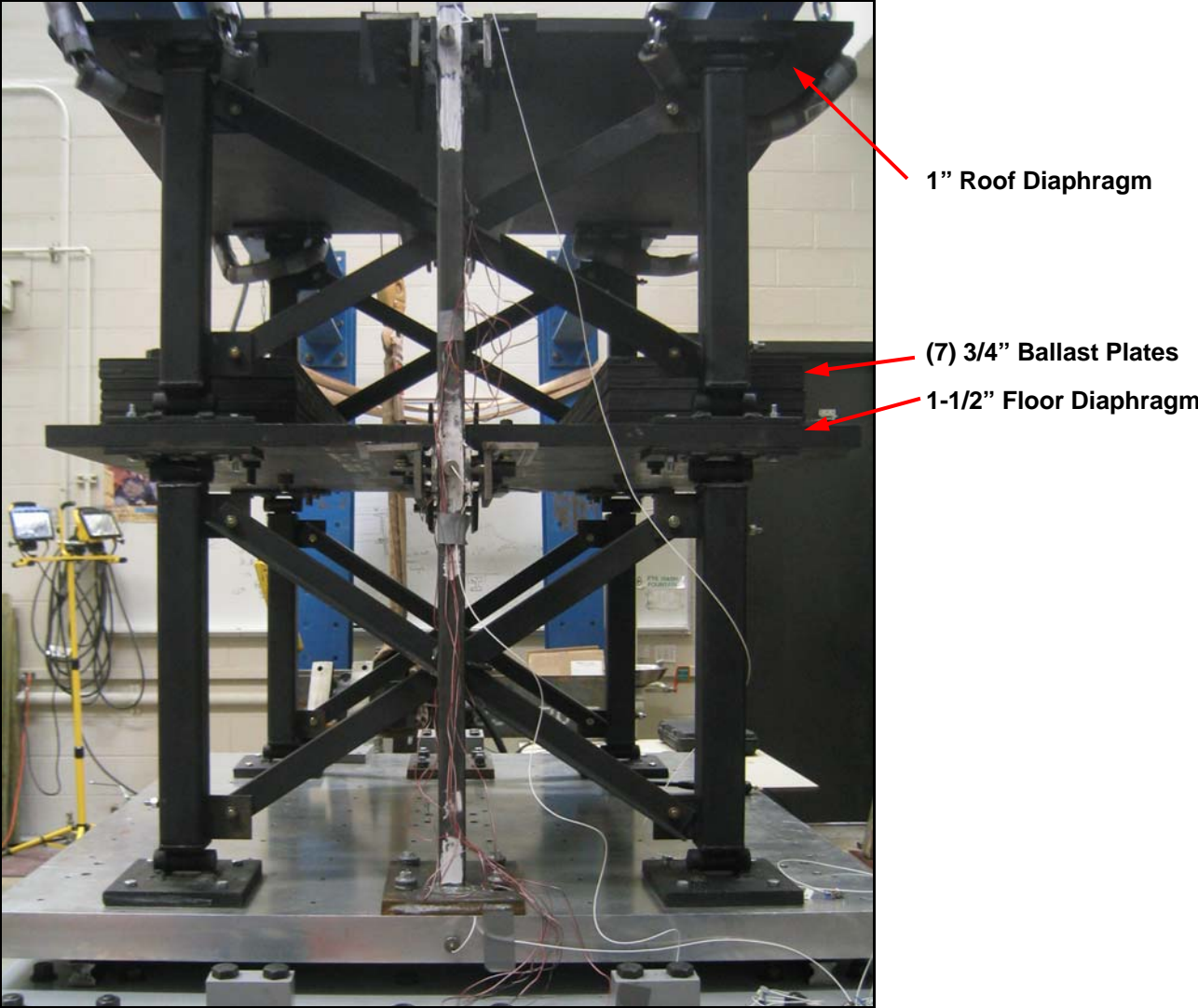


Figure 4. 8: Photograph of Leaner Frame – Side View

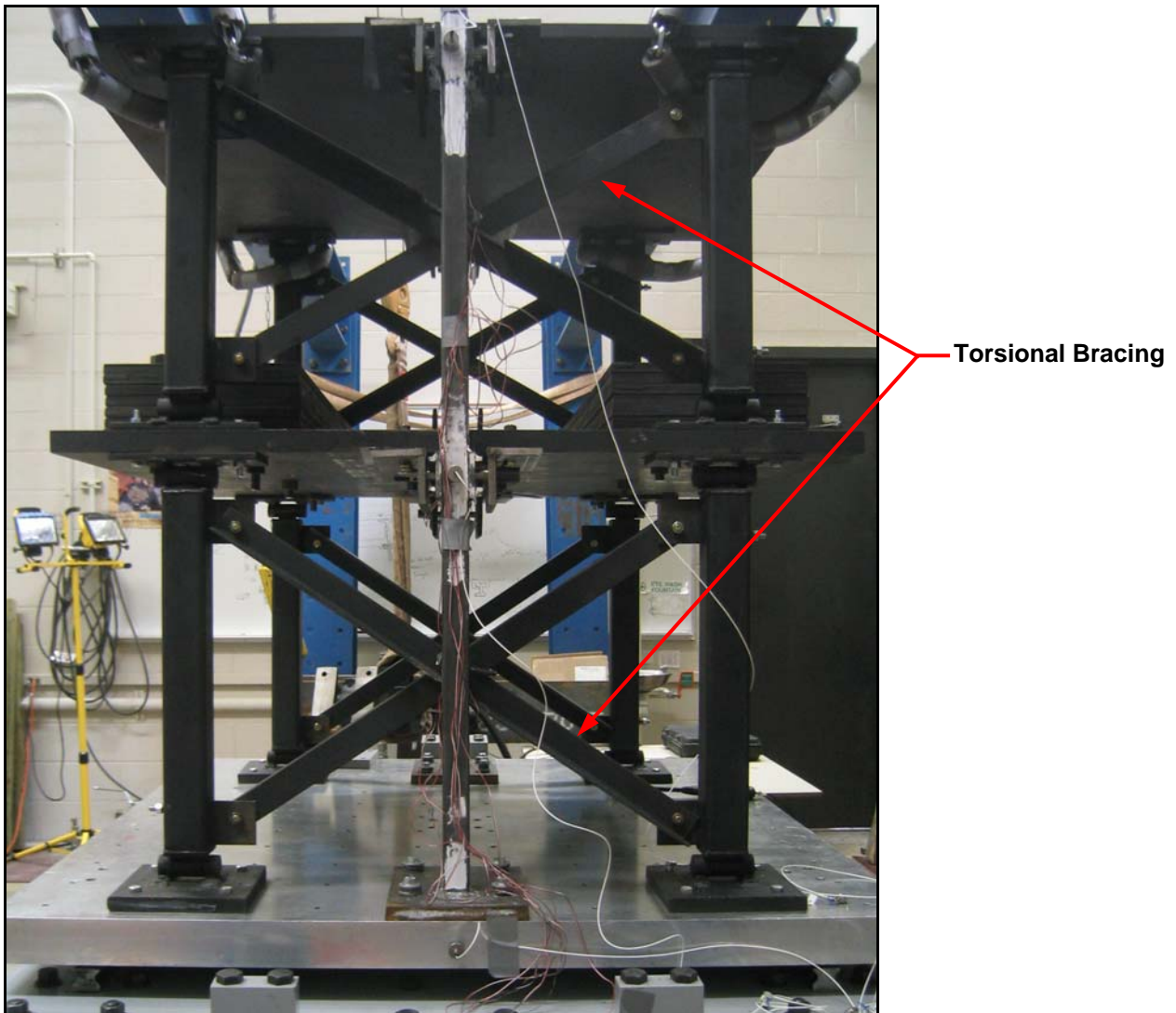


Figure 4. 9: Photograph of Leaner Frame – End View

### 4.3 FRAME 1 TESTING

#### 4.3.1 STIFFNESS TESTING

Quasi-static stiffness tests were conducted on Frame 1 to determine the lateral stiffness of the moment frame alone, and the lateral stiffness of the moment frame when connected to the auxiliary leaner frame. The test was conducted by applying a quasi-static load at the roof diaphragm level, while measuring the displacement at the load-point (Figure 4.10). Load was applied manually using a turnbuckle and measured using a 10,000-lb load-cell. Displacement was measured using a wire-type potentiometer. Two loading cycles were completed from 0 lb to 850 lb. Load and displacement were read manually using two portable, battery-powered strain

indicators. Readings for load and displacement were recorded manually at approximately 100-lb increments. Two loading cycles were conducted with the leaner frame engaged. The brackets, which connect the moment frame to the leaner frame, were then removed and two loading cycles were conducted on the moment frame only. Results for the loading cycles are shown in Figure 4.11.

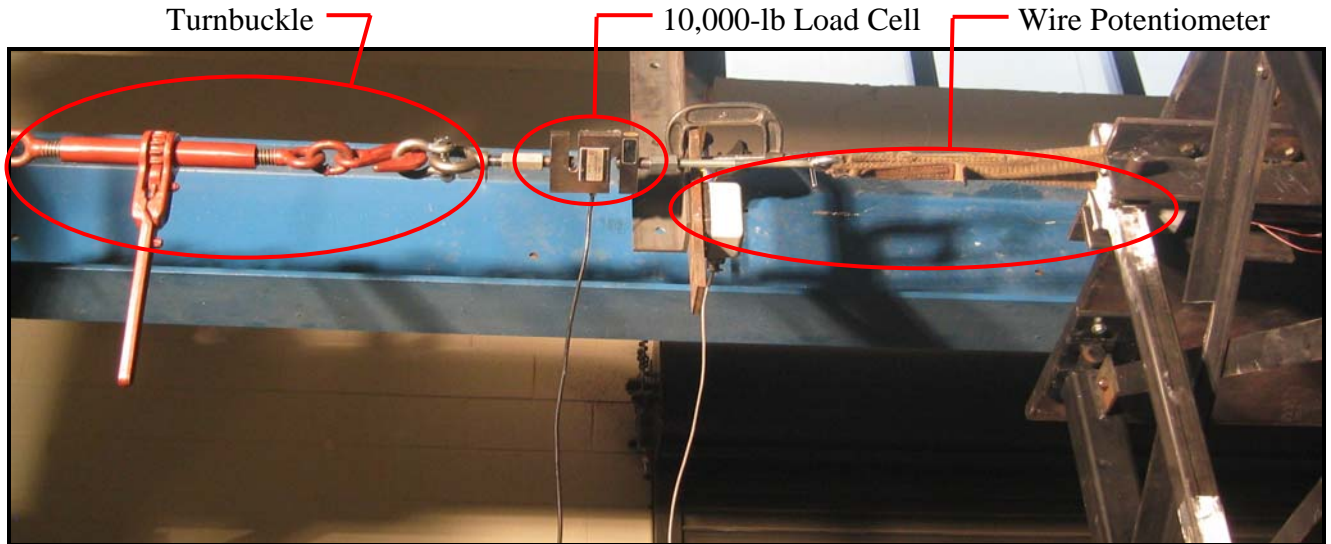


Figure 4. 10: Photograph of Stiffness Test

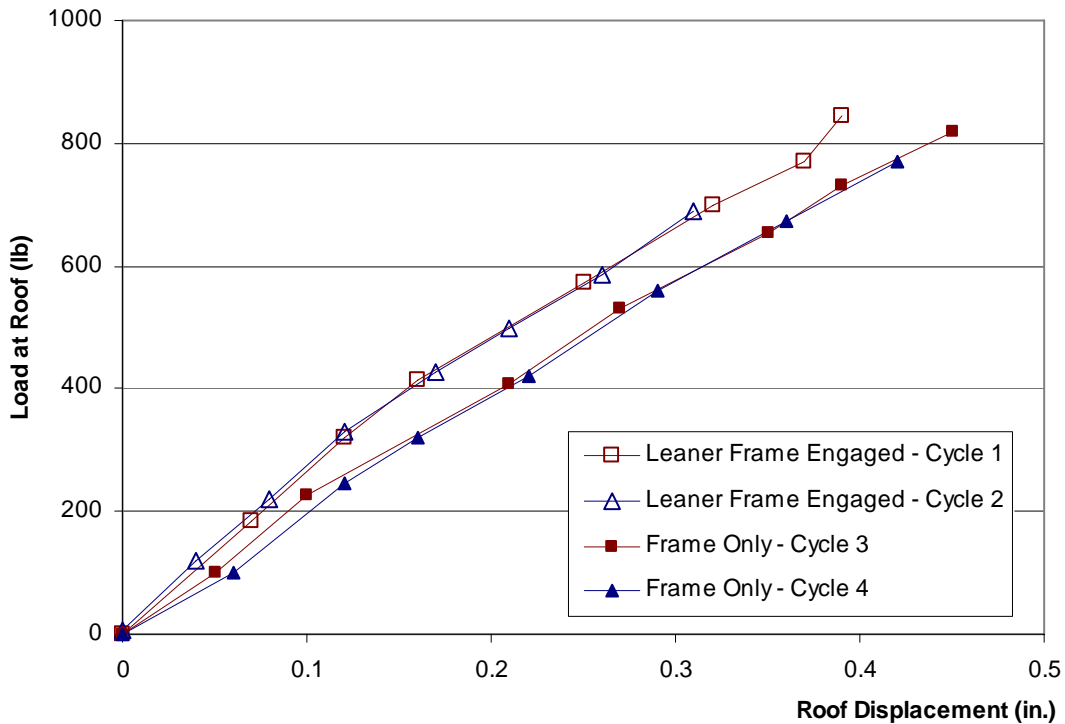


Figure 4. 11: Load vs. Displacement at the Roof (Stiffness Testing)

A linear regression was performed for data recorded during loading cycles 1 and 2, and for data from loading cycles 3 and 4 for displacements less than 0.3 in. (Figure 4.12). The stiffness calculated for the moment frame alone was equal to 2,000 lb per inch of roof displacement. The stiffness calculated for the total system with the leaner frame engaged was equal to 2,240 lb per inch of roof displacement. It should be noted that the decision to base the regression analyses on displacements less than 0.3 in. was based on the small amplitude of displacements observed at the roof during the sinusoidal testing described in Section 4.3.4. The results of the stiffness test of the moment frame without the leaner frame engaged allowed for a more accurate estimate of the contribution of the panel zones and the flange plates of the beam-to-column moment connections to the overall moment frame stiffness. In addition, a comparison of results between the stiffness test conducted with the leaner frame engaged and the stiffness test of the moment frame only was used to quantify the stiffness added to the total system by the leaner frame. Determining the lateral stiffness of the moment frame relative to the lateral stiffness of the total system with the leaner frame engaged allowed the moment frame to be effectively de-coupled from the leaner frame in the DRAIN model.

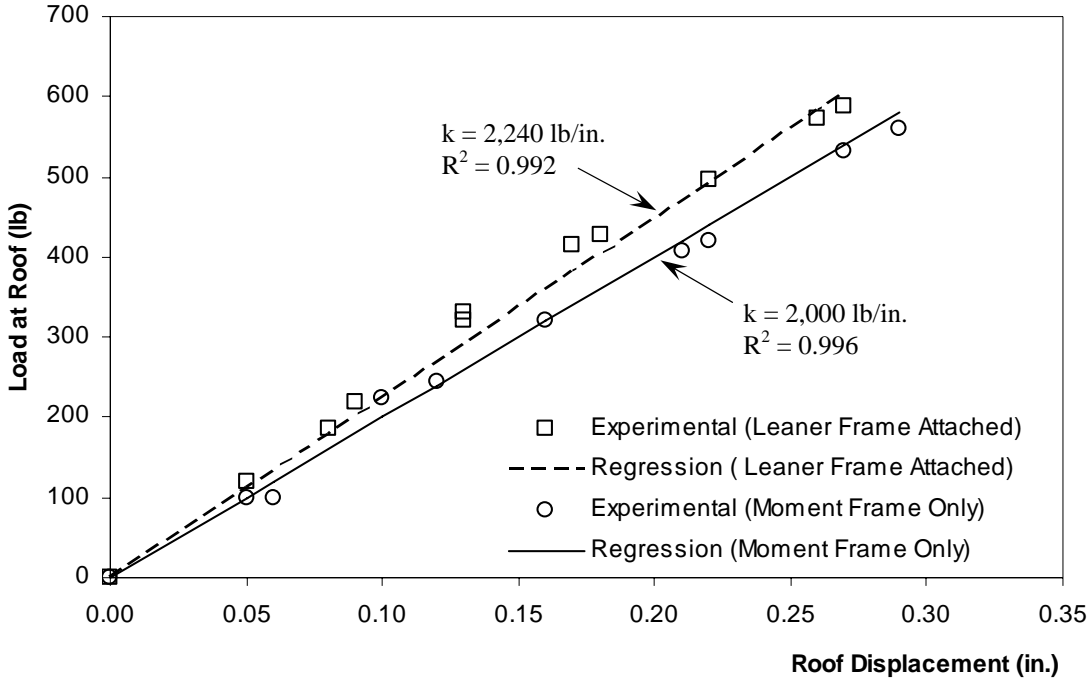


Figure 4. 12: Frame Stiffness Regression

### 4.3.2 DRAIN MODEL MODIFICATIONS BASED ON STIFFNESS TESTING

The DRAIN analyses used to proportion the 1:6-scale moment frame were completed prior to designing the beam-to-column moment connections for the frame (Figure 4.13). Consequently the bending stiffness added by the flange plates and doubler plates used for the connection, identified in Figure 4.13, were not included in the original analyses. As a result, the lateral stiffness of the actual moment frame was greater than modeled originally in DRAIN. The bending stiffness of elements at the beam-to-column interface was increased such that the displacement due to a point load at the roof in DRAIN matched the displacement of the roof due to the load applied during the stiffness tests of the moment frame without the leaner frame engaged.

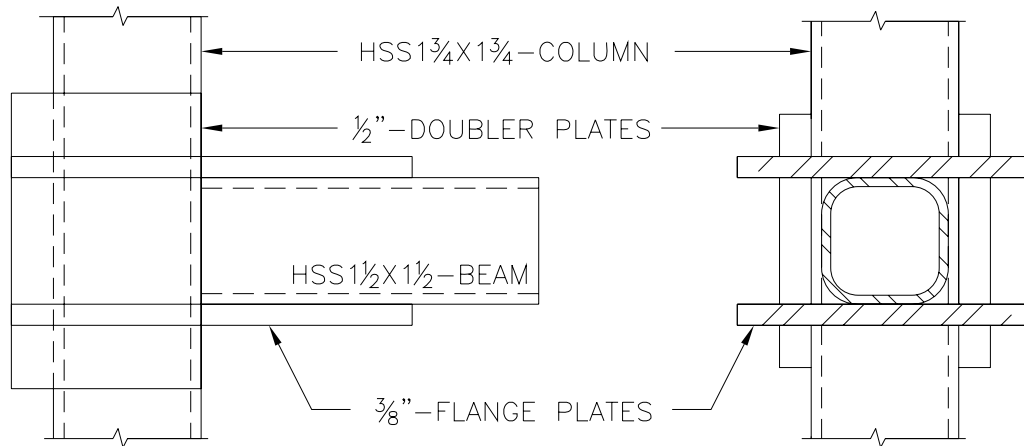


Figure 4. 13: Beam-to-Column Moment Connection Detail

A second source of stiffness, which was not accounted for in the original DRAIN model, was the leaner frame. Two components of the leaner frame contributed stiffness to the system: the hinges at the top and bottom of each column (Figure 4.14), and the zero-tolerance pin-connections between the diaphragms and the moment frame (Figure 4.15). As noted above, results of the stiffness test were used to quantify the stiffness added by the leaner frame to the overall system. Approximately 11% of the moment frame stiffness was added to the system by the leaner frame. Lateral stiffness added by the leaner frame was not considered insignificant, and in fact was likely to be greater than the relative amount of lateral stiffness contributed to the prototype building by non-lateral-force resisting frames. However, the objective of the project

was to determine the modification of frame response by the ropes. Since the stiffness added was consistent for Test 1 and Test 2, this was determined to be acceptable.

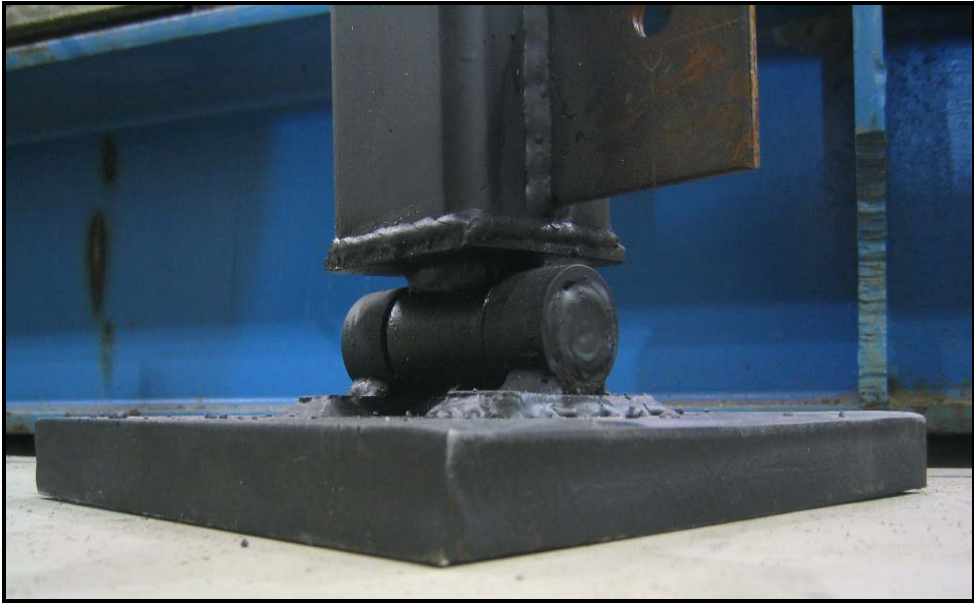


Figure 4. 14: Photograph of Column Hinge

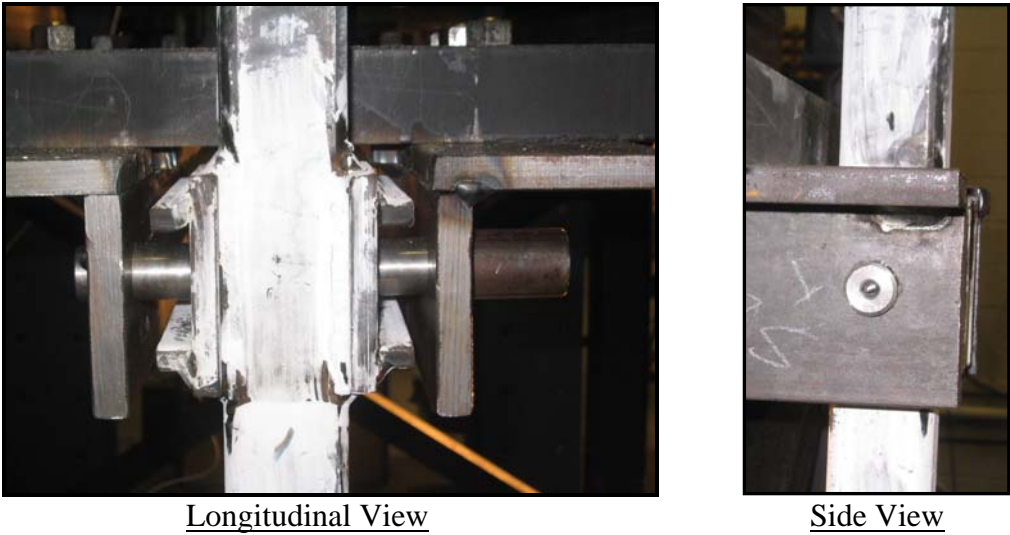


Figure 4. 15: Photographs of Zero-Tolerance Pin-Connections

To account for the additional stiffness due to the leaner-frame-pin-connections and zero-tolerance pins, the DRAIN model was modified by adding DRAIN Type-01 elements, described in Chapter 3, at the diaphragm levels as shown in Figure 4.16. The axial stiffness properties of the elements were proportioned such that the overall lateral stiffness of the analytical model matched the stiffness determined experimentally. The resulting first and second resonant frequencies of vibration of the analytical model were reasonably close to those determined in Section 4.3.4. Table 4.1 lists resonant periods of vibration for the prototype moment frame and the 1:6-scale moment frame prior to, and subsequent to, stiffness adjustments.

Table 4. 1: Comparison of Resonant Periods of Vibration

	<b>1:6-Scale Moment Frame Prior to Adjustment</b>	<b>1:6-Scale Moment Frame Subsequent to Adjustment</b>
<b>T<sub>1</sub> (seconds)</b>	0.29	0.25
<b>T<sub>2</sub> (seconds)</b>	0.09	0.09

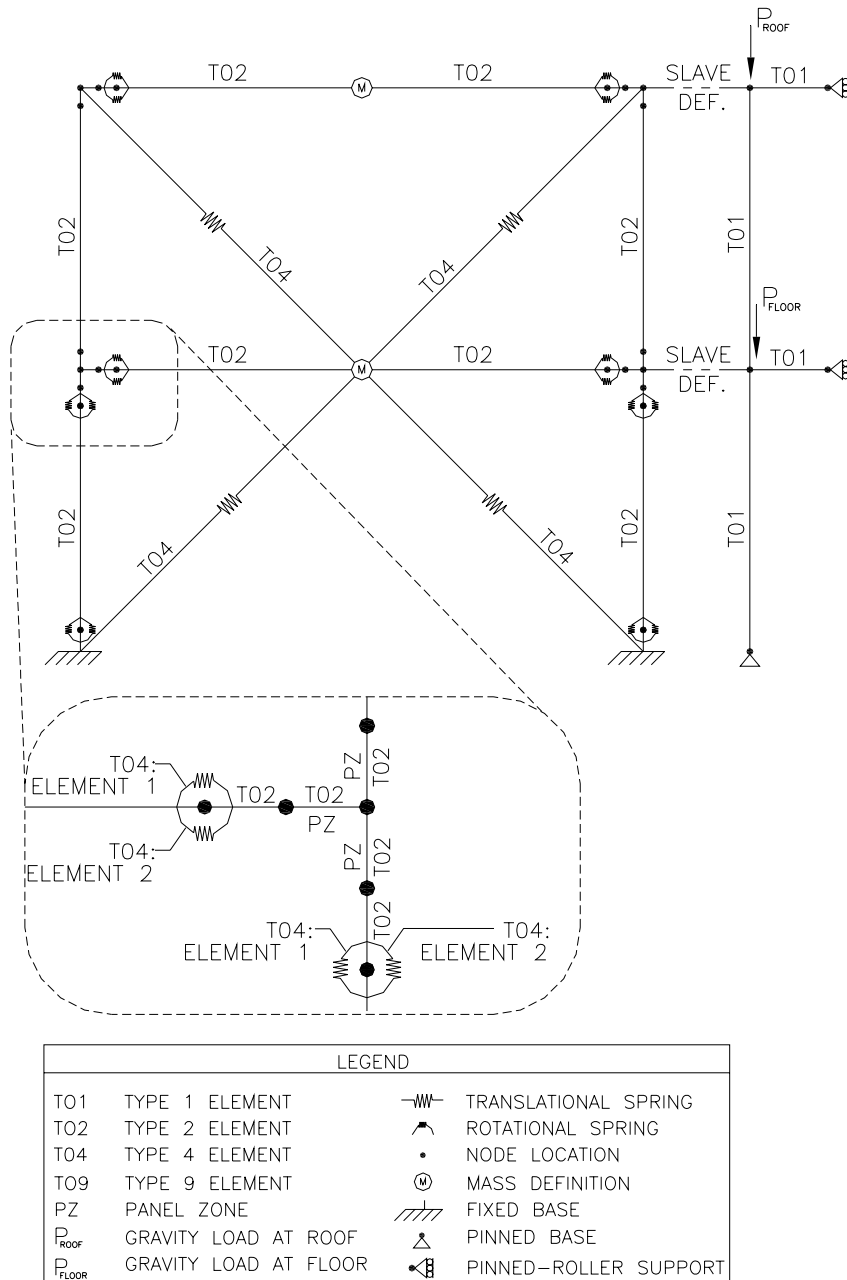


Figure 4. 16: DRAIN Element Usage Diagram with Leaner-Frame Stiffness Added

### 4.3.3 IMPACT-HAMMER TESTING

Impact-hammer tests were conducted to determine the lateral resonant frequencies of vibration for the 1:6-scale shaking table. A calibrated impact hammer was used to provide impulse input (Figure 4.17). Two *PCB-Piezotronics* seismic accelerometers were used to

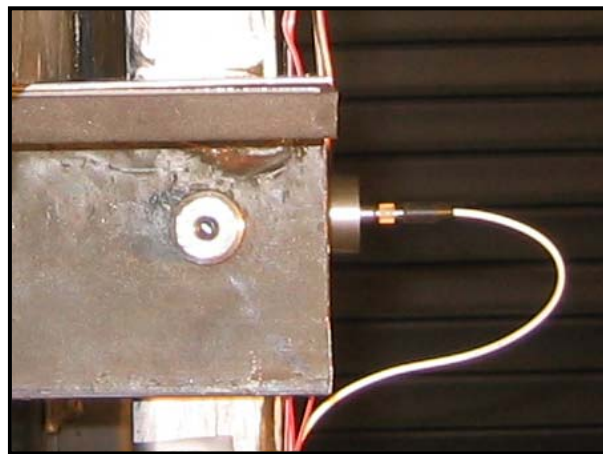
measure acceleration at each diaphragm level (Figure 4.18). Voltages from the impact hammer and accelerometers were recorded and post-processed using a *Spectral Dynamics*, SigLab dynamic signal analyzer and spectral analysis software. Power to the accelerometers was provided by a signal conditioner, internal to the SigLab unit.



Figure 4. 17: Photograph of Impact Hammer



Seismic Accelerometer  
Source: www.PCB.com



Typical Accelerometer Location

Figure 4. 18 Photograph of Accelerometer

Tests were conducted by striking the experimental frame at the floor diaphragm level using the impact hammer in the direction of shaking-table motion. The impulse input from the hammer and the resulting accelerations at the floor and roof level were recorded. An 80-second record was taken for each of three successive strikes with the hammer. The 80-second record allowed for frequency content to be recorded between 0 Hz and 20 Hz at 0.0125-Hz frequency

resolution. Repeating the procedure three times allowed for computation of coherence between the reference input, or impulse load from the hammer strike, and the resulting response of the system. This procedure was repeated for hammer strikes at the roof diaphragm level as well.

A typical impulse from the impact hammer is plotted in Figure 4.19. Normalized frequency response functions for the roof and floor response, corresponding to the floor level strike, are plotted in Figure 4.20. The frequency response functions were normalized by dividing the function at each frequency by the maximum value, calculated at the first resonant frequency. Coherence functions are plotted in Figure 4.21. Note that the peak values for the transfer functions were observed at 4.67 Hz and 13.03 Hz for the floor and roof responses. The coherence value corresponding to these frequencies was greater than 0.995 for both frequencies at the floor and roof levels. Peaks in floor and roof transfer functions were recorded at identical frequencies, with similar coherence at those frequencies when the frame was struck at the roof level diaphragm.

The first and second resonant frequencies observed during impact-hammer testing were 13% and 9% higher than those calculated using the DRAIN model with modifications described in Section 4.3.2. One possible explanation was stiffness added by the column hinges and zero-tolerance pin connections due to static friction associated with the rotational degree of freedom, which was not overcome in the impact-hammer test. Since the impulse load from the hammer was extremely small in comparison to inertial loading expected on the 1:6-scale frame, resulting lateral translation was nearly zero and no rotation was seen in the column hinges or zero-tolerance pin connections. Resistance to initial rotation in the hinges and pins during impact-hammer testing was hypothesized to result in higher resonant frequencies and lower damping when compared to the dynamic response of the system after hinge and pin friction was overcome. In fact, lower resonant frequencies and greater damping were observed during low-amplitude sinusoidal testing, during which free rotation was clearly visible in column hinges and zero-tolerance pins. Therefore, no adjustments were made to the DRAIN model based on impact-hammer testing.

Impact-hammer testing was useful in identifying two distinct resonant frequencies between 0 Hz and 20 Hz. The values for the resonant frequencies determined during impact-hammer testing were also useful in identifying the resonant frequencies during low-amplitude

sinusoidal testing, and verifying that no additional resonant frequencies exist in the range of frequency considered.

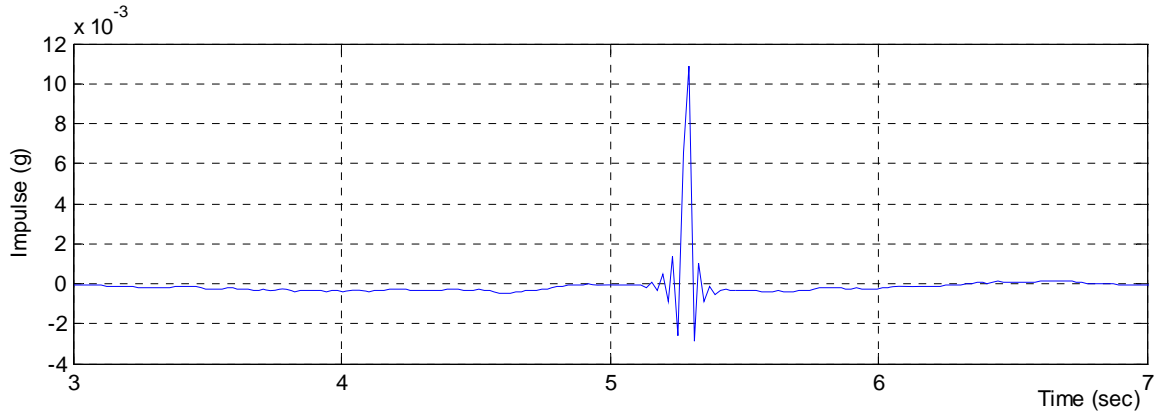


Figure 4.19: Typical Impulse from Impact-Hammer Strike (Frame 1)

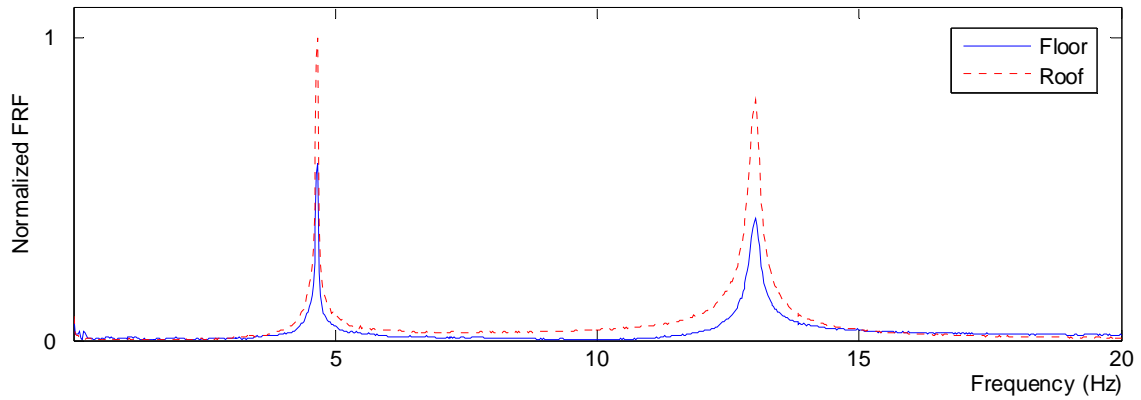


Figure 4.20: Roof and Floor FRF Response for Floor-Level Impulse (Frame 1)

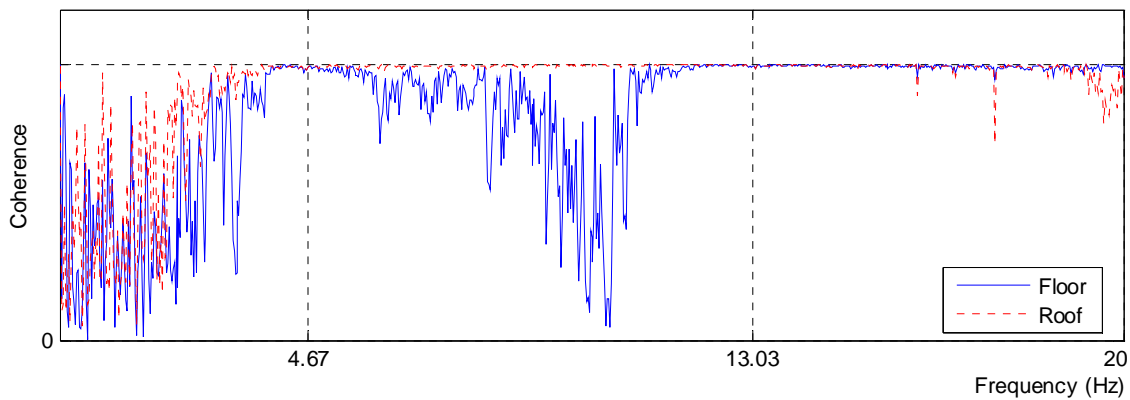


Figure 4.21: Coherence between Impulse and Floor and Roof Response for Floor-Level Impulse (Frame 1)

#### 4.3.4 LOW-AMPLITUDE SINUSOIDAL GROUND MOTION TESTING

To determine the resonant frequencies and damping of the 1:6-scale frame with amplitudes of displacement large enough to overcome static friction in the leaner-frame hinges and zero-tolerance pins, the frame was excited with low-amplitude sinusoidal ground motion input using the shaking table. Low-amplitude refers to the displacement amplitude of the sinusoidal loading function, and can be interpreted to mean less than 0.025 in. Throughout the test, floor and roof level accelerations were measured and recorded using the equipment described in Section 4.3.2. Shaking-table acceleration was measured using a third *PCB Piezotronics* seismic accelerometer. Shaking-table displacement was measured using a linear displacement voltage transducer internal to the shaking table actuator.

To find resonant frequencies experimentally, an operating deflection shape (ODS) (Richards, 1997) was determined based on roof acceleration, referenced to shaking-table acceleration for frequencies between 0 Hz and 20 Hz. To plot the ODS FRF, the shaking table was excited at 50 frequencies. For each frequency, an 80-second time record was captured subsequent to the system reaching steady-state vibration. A transfer function between table acceleration and roof acceleration was calculated at 0.025-Hz increments, and the value of the transfer function at the excitation frequency was recorded. Frequencies near resonance were chosen at a closer interval than frequencies away from resonance to pinpoint the resonant frequency and to insure an accurate shape of the ODS FRF near resonant frequencies (Figure 4.22). ODS FRF results were normalized based on the largest value at the first resonant frequency. Peak values for the normalized ODS FRF correspond to the resonant frequencies of the system and were found to be approximately 4.3 Hz and 11.9 Hz for the first and second modes, respectively.

The FRF calculated at the roof level, referenced to the impact-hammer input, was plotted for comparison. As expected, the resonant frequencies determined during the low-amplitude sinusoidal testing were lower than those determined during the impact-hammer testing. Based on the relatively smaller slope of the ODS FRF in comparison to the impact-hammer FRF on either side of the resonant frequencies, it was also determined that damping was greater during the low-amplitude sinusoidal testing.

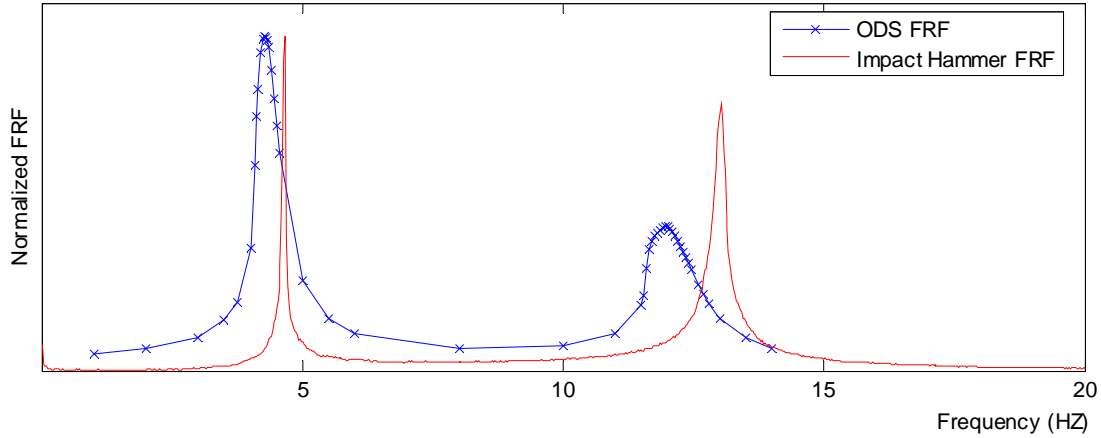


Figure 4. 22: Comparison of Normalized FRF's

To determine estimates for damping at each resonant mode of vibration, the experimental frame was shaken at the fundamental frequency until reaching steady-state and then allowed to decay. The resulting roof displacements were normalized by dividing all recorded displacement values by the greater of the maximum and the absolute value of the minimum values (Figure 4.23). An analytical model for viscous damping was calculated for comparison with the experimentally measured decay.

The following model was used to calculate decay of a viscously damped system for values of the damping ratio,  $\zeta$ , equal to 0.01, 0.02, and 0.03:

$$u_{i+1} = \frac{u_i}{e^{\delta}} \quad (4-1)$$

where  $u_i$  is the amplitude of roof displacement of the  $i^{\text{th}}$  cycle,  $u_1 = 1.0$ , and  $\delta$  is the logarithmic decrement:

$$\delta = \frac{2\pi\zeta}{\sqrt{1-\zeta^2}} \quad (4-2)$$

Values for roof displacement amplitude in successive cycles were calculated until the roof displacement was effectively equal to zero. Results for decay using the viscous damping model were plotted with the roof displacement decay trace for comparison (Figure 4.24). It can be seen that the damping of the system was higher at larger amplitude motion, when compared to the damping model used, indicating nonlinear damping. To investigate non-linear damping further, successive peaks from the normalized displacement trace was plotted in natural log scale from the beginning of decay at 30 cycles to 62 cycles of frame response (Figure 4.25).

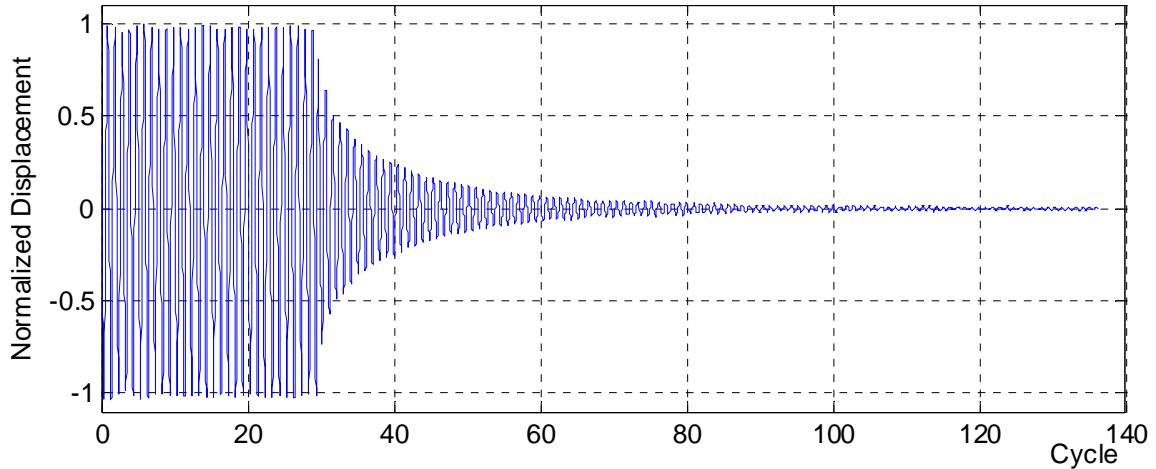


Figure 4. 23: Normalized Roof Displacement Decay (Frame 1, 4.3 Hz)

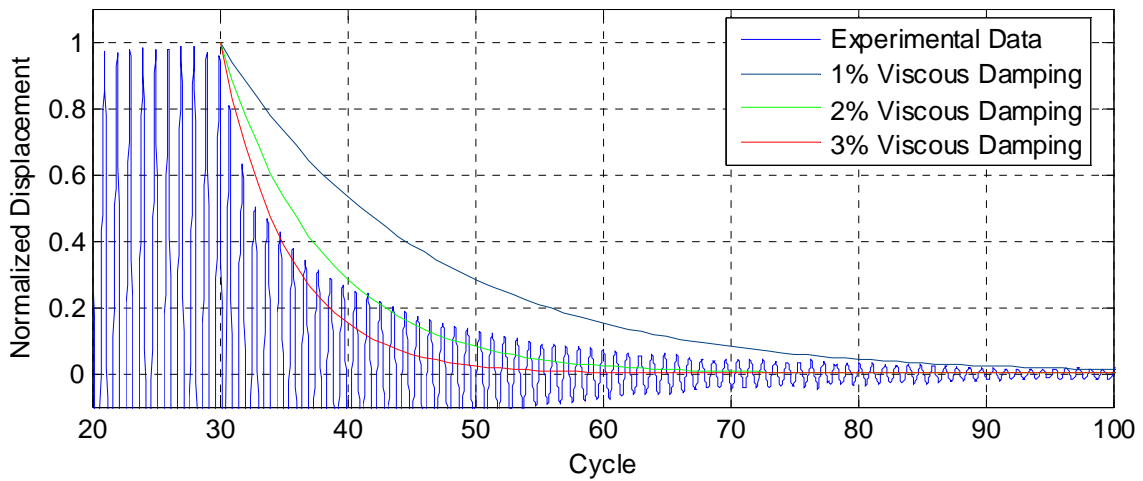


Figure 4. 24: Comparison of Roof Displacement Decay with Viscous Damping Model (Frame 1, 4.3 Hz)

Three distinct magnitudes of damping were indicated by shifts in the slope between successive peaks. A regression of successive peak natural log normalized displacement values was calculated for each of the three distinct damping values. The resulting regression lines are shown in Figure 4.25, and are indicated as R1, R2, and R3. The slope of the regression is the log decrement,  $\delta$ , defined in Equation 4.2 above. The damping ratio was found by re-arranging Equation 4.2, and the percent-viscous damping was calculated as follows:

$$\zeta = \frac{\delta}{\sqrt{2\pi^2 + \delta^2}} \quad (4-3)$$

$$\% \text{ Viscous Damping} = \zeta (100\%) \quad (4-4)$$

Regression results and resulting percent viscous damping values are presented in Table 4.2. The damping was found to range between 3.49% at higher levels of roof displacement to 0.75% at extremely low levels of frame displacement.

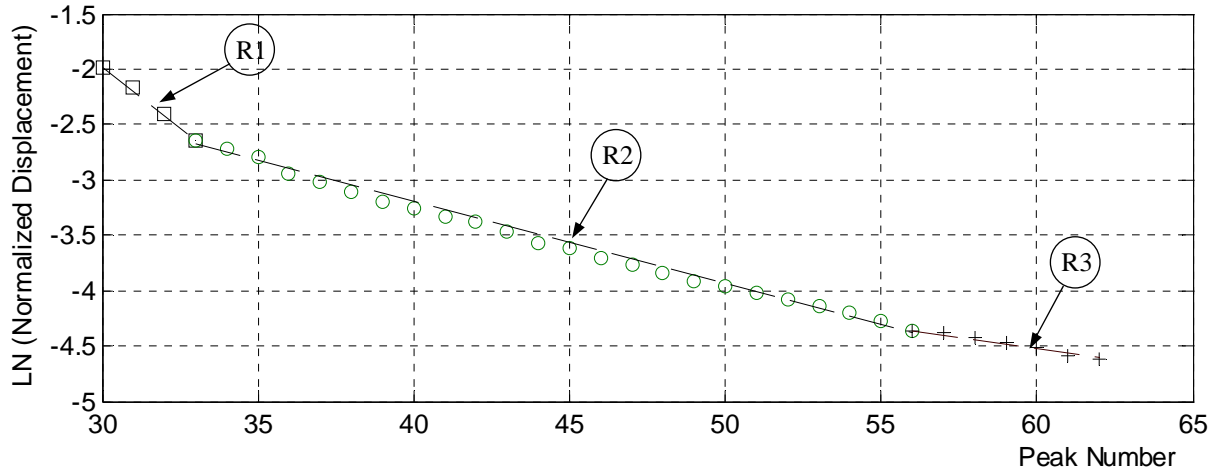


Figure 4. 25: Estimate of Log Decrement for Non-Linear Damping at Roof

Table 4. 2: Estimated Damping and Regression Statistics for Estimating Log Decrement

Level	Regression Number	Log Decrement ( $\delta$ )	$R^2$	% Viscous Damping
Roof	1	0.219	0.994	3.49
	2	0.073	0.994	1.16
	3	0.047	0.981	0.75

Damping was primarily attributed to rotational friction present in the leaner-frame hinges and zero-tolerance pin connections. Although damping was considered to be large with respect to inherent damping in steel structures, typically assumed to be less than 2% of critical damping, the friction in the hinges and pins was determined to be representative of damping inherent in steel frame structures. Further, the objective of the project was to determine the modification of frame response by the ropes. Since damping was consistent for Test 1 and Test 2, this was determined to be acceptable.

It should be noted that the shaking-table actuator may have also contributed to the decay of the roof drift trace. Extremely small motion of the actuator, subsequent to terminating sinusoidal base input may have occurred. As a result hydraulic fluid would have been driven through internal orifices of the actuator. Although no movement was visually noticeable subsequent to terminating the command signal, imperceptible motion could have occurred, resulting in slight over-representation of structural damping.

The structure was also shaken at the second resonant frequency. The normalized roof displacement was plotted (Figure 4.26), and the viscous damping model was plotted over the roof displacement decay trace (Figure 4.27). An effective viscous damping of the system was estimated to be approximately 2% in the second mode.

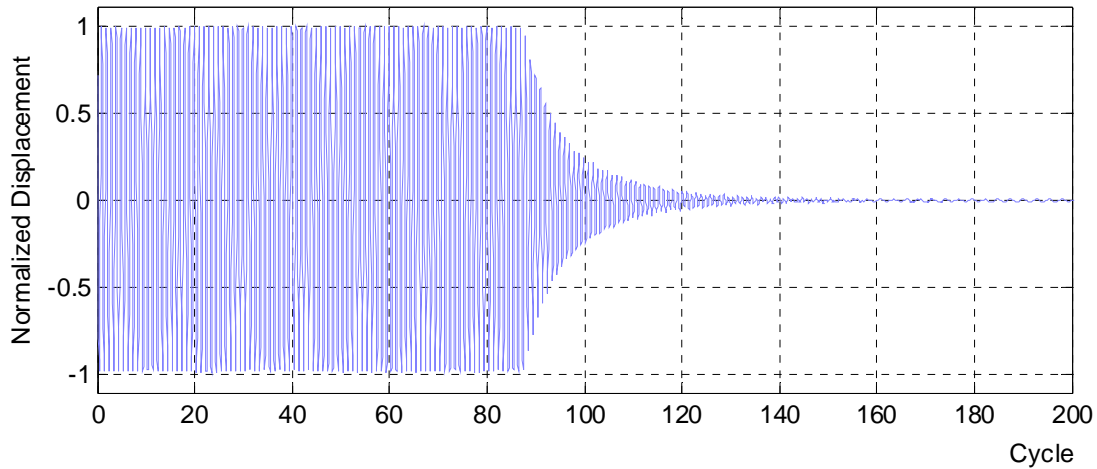


Figure 4. 26: Normalized Roof Displacement Decay (Frame 1, 11.9 Hz)

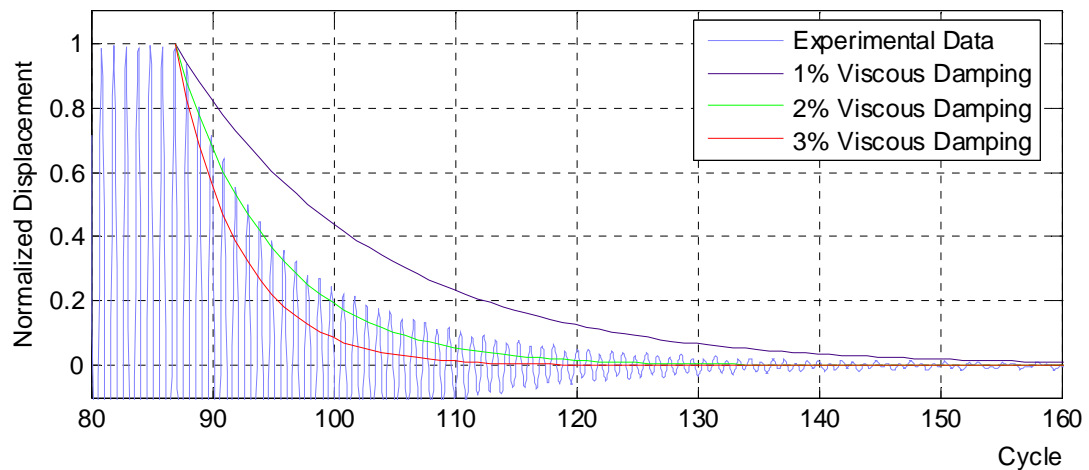


Figure 4. 27: Comparison of Roof Displacement Decay with Viscous Damping Model (Frame 1, 11.9 Hz)

#### 4.3.5 DRAIN MODEL MODIFICATIONS BASED ON SINUSOIDAL GROUND MOTION TESTING

The stiffnesses of the auxiliary linear springs added to the DRAIN model at the floor and roof levels were proportioned such that the system: 1) had a lateral stiffness that remained consistent with the lateral stiffness determined experimentally, and 2) had first and second resonant frequencies that were reasonably close to those found experimentally. Upon making adjustments to the DRAIN model, the first and second resonant frequencies were calculated to be 4.24 Hz and 12.0 Hz, respectively. These are plotted over the ODS FRF for comparison in Figure 4.28.

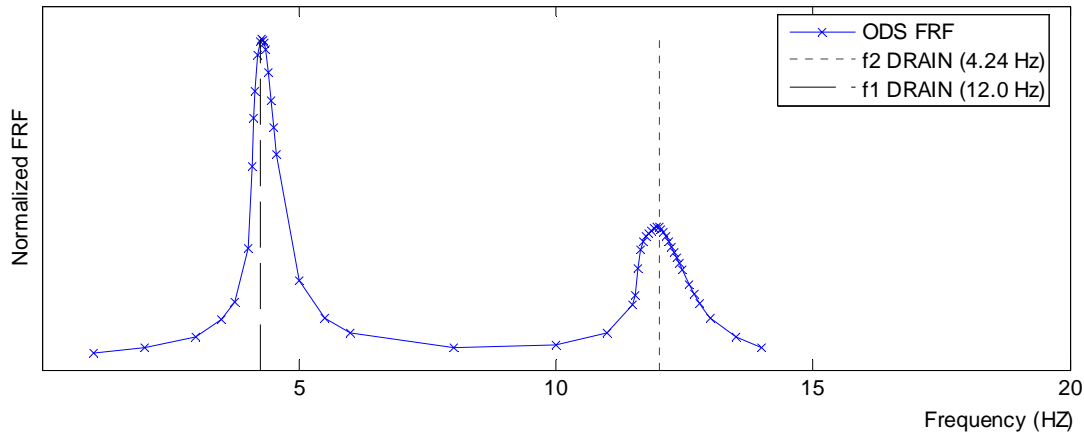


Figure 4. 28: Resonant Frequencies Calculated Using DRAIN and ODS FRF

Based on the low-amplitude sinusoidal testing and decay from steady state at resonance, equivalent viscous damping was defined as 2.5% of critical damping in the DRAIN model. The DRAIN model was then excited by simulating the acceleration input used to excite the frame experimentally at 4.3 Hz. The DRAIN model was allowed to reach steady state and then vibrate freely. Displacements and accelerations were recorded at the roof and floor and were plotted with experimental roof and floor drift traces (Figures 4.29 through 4.32).

Correlation between maximum floor displacement for DRAIN and experimental results was good, while correlation of the decay trace was poor throughout decay. Correlation between maximum roof displacement for DRAIN and experimental results was fair, with good correlation for decay at displacement values above 0.02 in., and poor for decay below 0.2 in. of displacement. Difficulty in matching all aspects of the decay trace at the roof and floor was attributed to simplified damping definitions in DRAIN. The method of defining damping in DRAIN consists of defining coefficients for stiffness proportional damping of each element, and mass proportional

damping for each nodal mass definition. DRAIN does not allow for nonlinear damping definitions in the elements used for this model. Since the damping of the 1:6-scale moment frame was nonlinear and appeared to increase at higher amplitudes of motion, the simplified method for defining damping in DRAIN was not effective in estimating damping at all levels of motion. It was determined that the correlation at large- amplitude motion was more important than at the low-amplitude motion. Since fair to good correlation was evident at the higher amplitude displacement, the damping definition was determined to be adequate.

The sensitivity of the DRAIN model to damping for the shaking table experiment was also investigated by exciting the frame with the Northridge ground motion, and varying the level of equivalent viscous damping, defined as 1%, 2%, and 3% of critical viscous damping. The resulting peak amplitudes for displacement, acceleration, and base shear did not change by more than 3%. Decay of the response subsequent to the initial pulses of the event was more sensitive. This study was primarily concerned with modification to peak response of displacement, acceleration, and base shear. It was therefore determined that the DRAIN model was adequate for predicting the dynamic, elastic response of the experimental frame when subjected to displacement input at the base with the simplified damping definitions allowed in DRAIN.

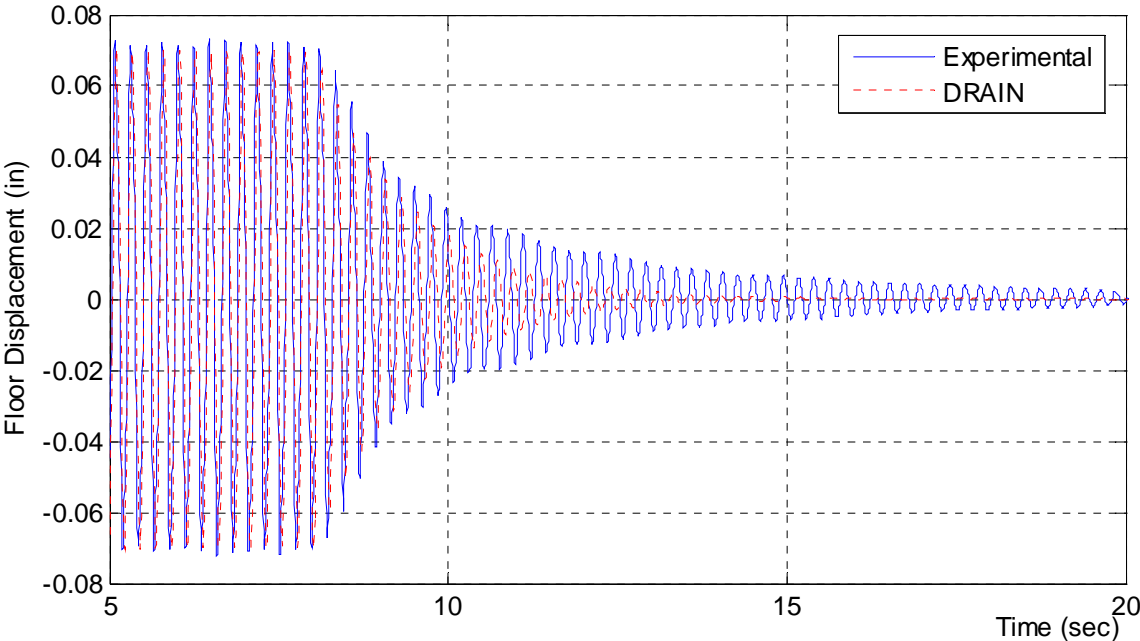


Figure 4. 29: Floor Displacement Decay Comparison (Frame 1, 4.3 Hz)

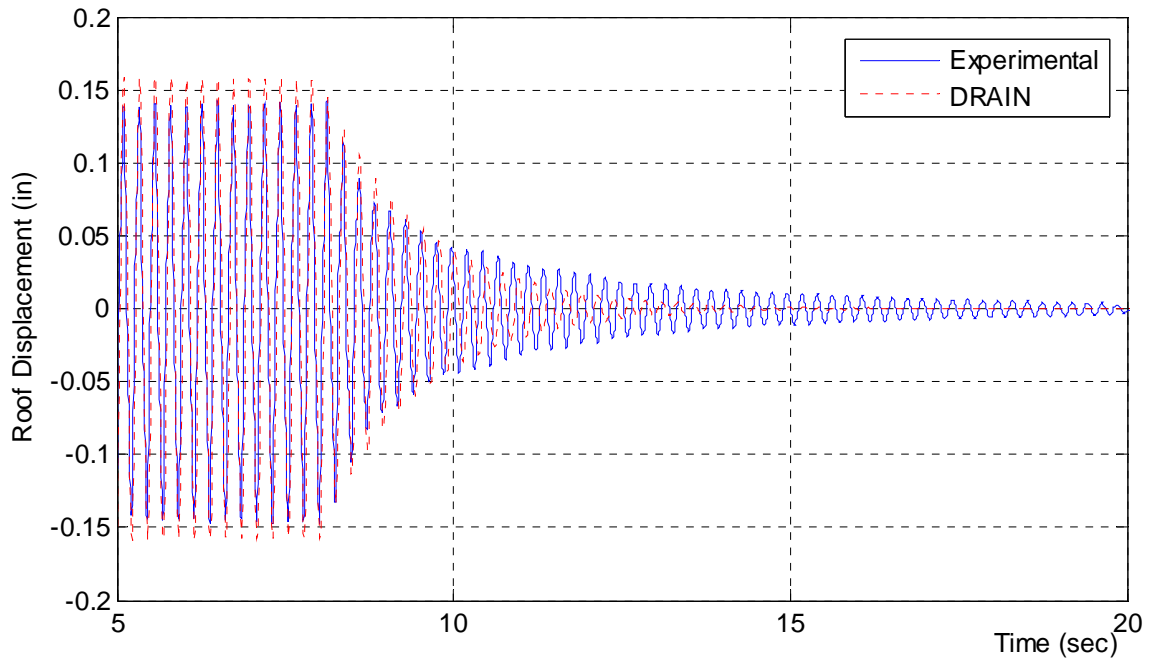


Figure 4. 30: Roof Displacement Decay Comparison (Frame 1, 4.3 Hz)

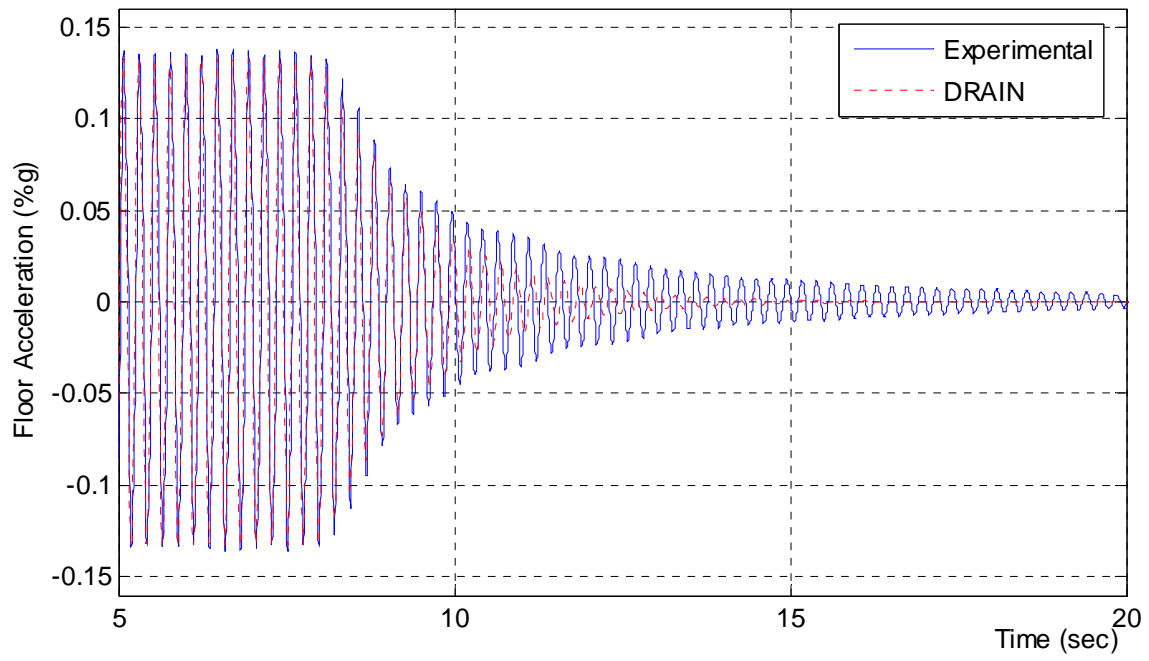


Figure 4. 31: Floor Acceleration Comparison (Frame 1, 4.3 Hz)

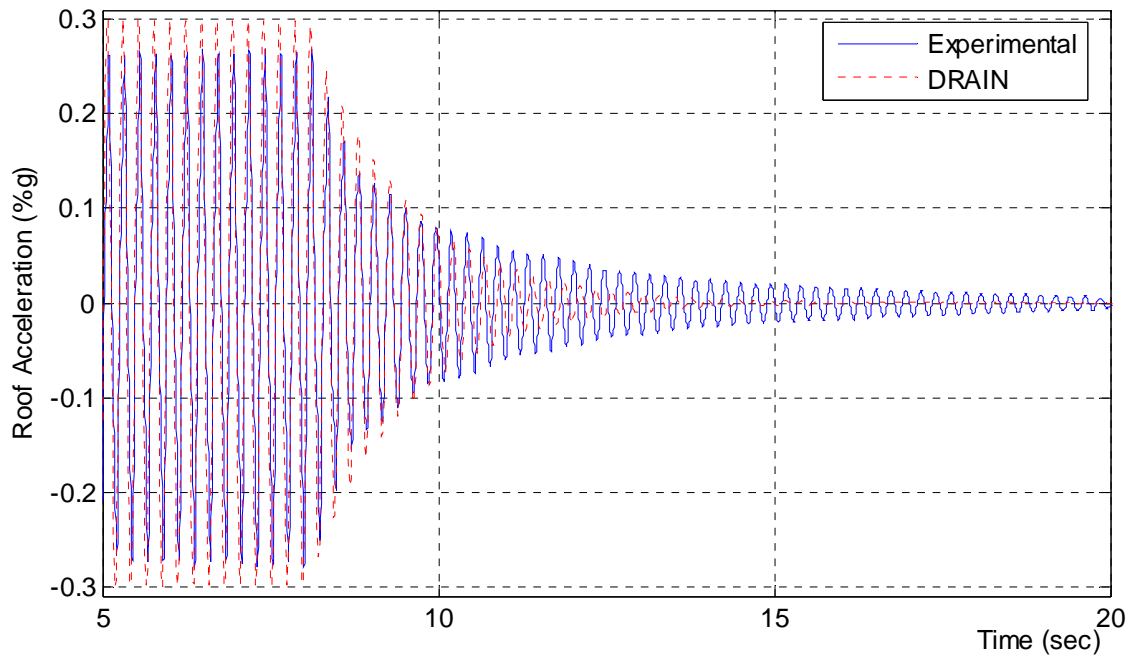


Figure 4.32: Roof Acceleration Comparison (Frame 1, 4.3 Hz)

#### 4.4 FRAME 2 TESTS

Frame 2 designates the second moment frame used for Northridge ground-motion testing described in Chapter 5, in which ropes were added. Since the ultimate goal of the ground-motion tests was to demonstrate the improvement of performance of the steel moment frame when ropes were added, it was important to demonstrate that Frame 1 was nearly identical to Frame 2. Through the use of stiffness testing and modal testing, the elastic stiffness, pre-yield resonant frequencies of vibration, and damping of the moment frames, when fit-up with the leaner frame on the shaking table, were shown to be acceptably similar. The results of these tests conducted using Frame 2 and the comparison of test results for Frame 1 and Frame 2 are presented in this section.

It should be noted that material properties of the frame could not be compared without the use of destructive testing. However, great care was taken to ensure that fabrication techniques of the frames were identical, and that differences in the frame resulting from fabrication tolerances were minimized. As described in Section 4.1, to ensure that material properties for both frames were identical, beams for both frames were taken from the same heat of steel, as were columns,

flange plates, doubler plates, and base plates. To ensure that the geometry of each frame was as similar as possible, a jig was constructed for fit-up and welding of the moment frames.

#### 4.4.1 STIFFNESS TESTING

Stiffness tests, described in Section 4.3.1, were conducted on Frame 2 with the leaner frame engaged. Two loading cycles were completed and load and displacement were measured at approximately 100-lb intervals. The results of Frame 2 stiffness tests are shown with results of the Frame 1 stiffness tests, conducted with the leaner frame engaged, in Figure 4.33. The comparison chart of loading cycles indicates that the elastic stiffness of each system is very similar.

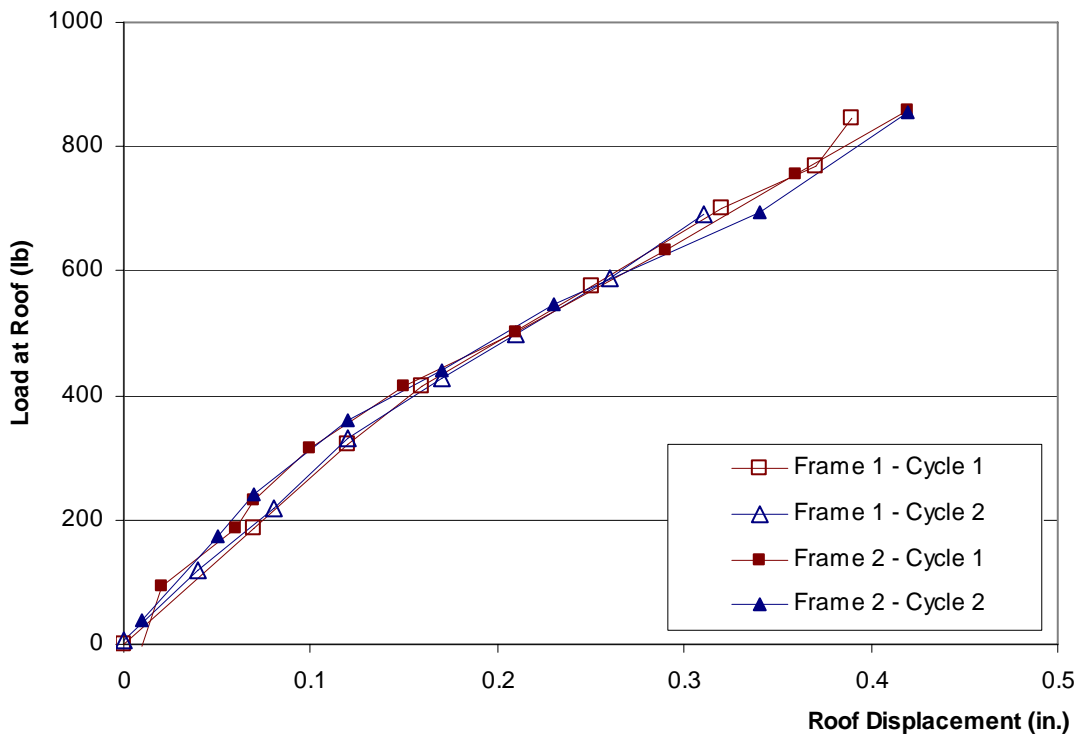


Figure 4. 33: Comparison of Stiffness Test Results: Frame 1 vs. Frame 2

#### 4.4.2 IMPACT-HAMMER TESTING

Impact-hammer testing was repeated on the experimental model with Frame 2 installed into the leaner frame. The same testing protocol, accelerometer measurement settings, and equipment described in Section 4.3.3 were used to test Frame 2. The impulse recorded, normalized floor and roof FRF comparisons, and coherence corresponding to the floor strike are

shown in Figures 4.34, 4.35, and 4.36, respectively. FRF's were observed to have two distinct peaks at 4.53 Hz and 12.68 Hz. The coherence value corresponding to these frequencies was greater than 0.995 for both frequencies at the floor and roof levels. Results correlating to the impulse at the roof were very similar.

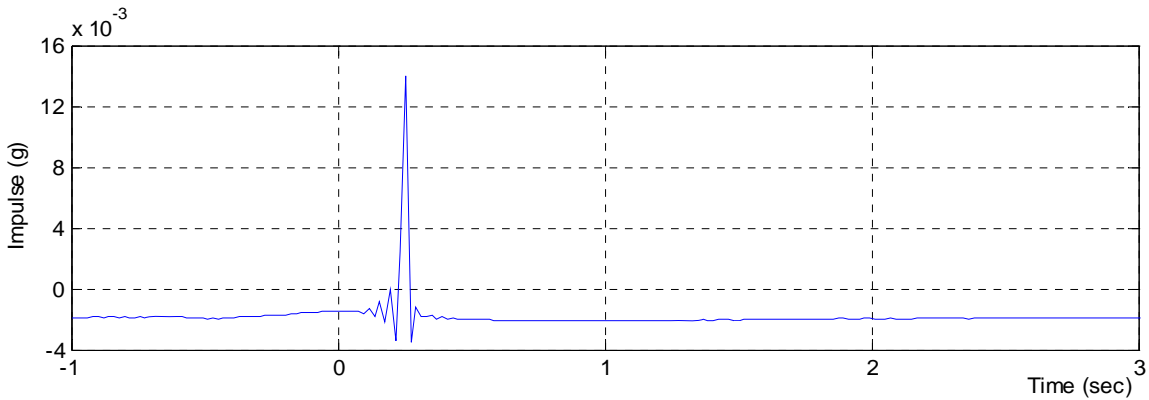


Figure 4.34: Impulse from Impact-Hammer Strike (Frame 2)

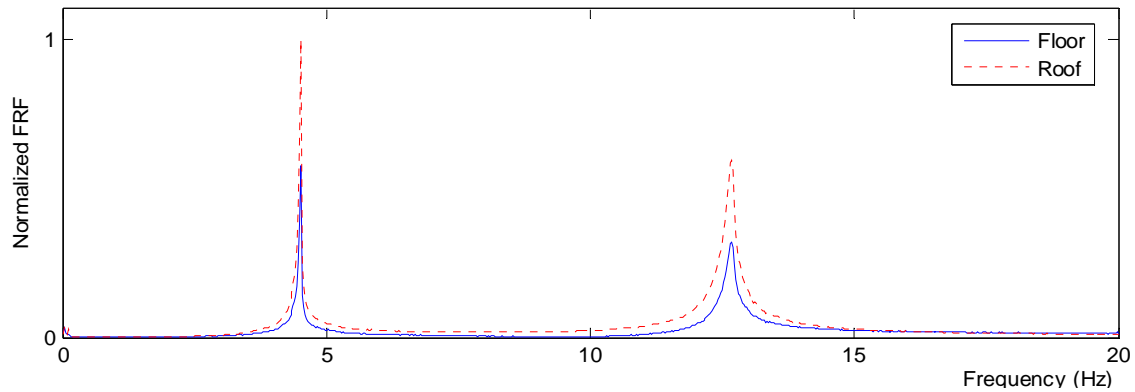


Figure 4.35: Roof and Floor FRF for Floor-Level Impulse (Frame 2)

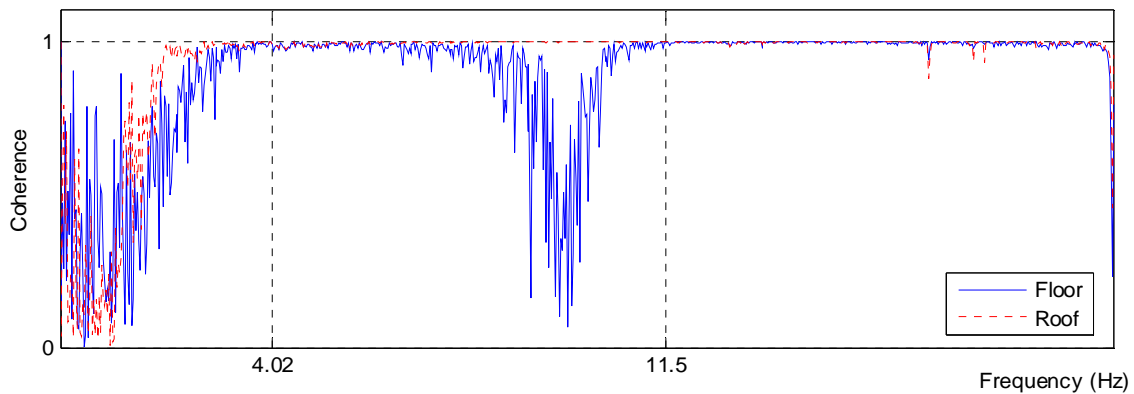


Figure 4.36: Coherence between Impulse and Floor and Roof Response for Floor-Level Impulse (Frame 2)

A comparison of normalized FRF's at the roof for Frame 1 versus Frame 2 is shown in Figure 4.37. The first and second resonant frequencies for Frame 2 were 3% and 2.5% lower than those measured for Frame 1. The shapes of the FRF's were also very similar. The similarity between the shapes and peaks of the FRF's for each frame during the impact hammer test indicated that the initial dynamic response of the frames would be the same when subjected to ground motion input.

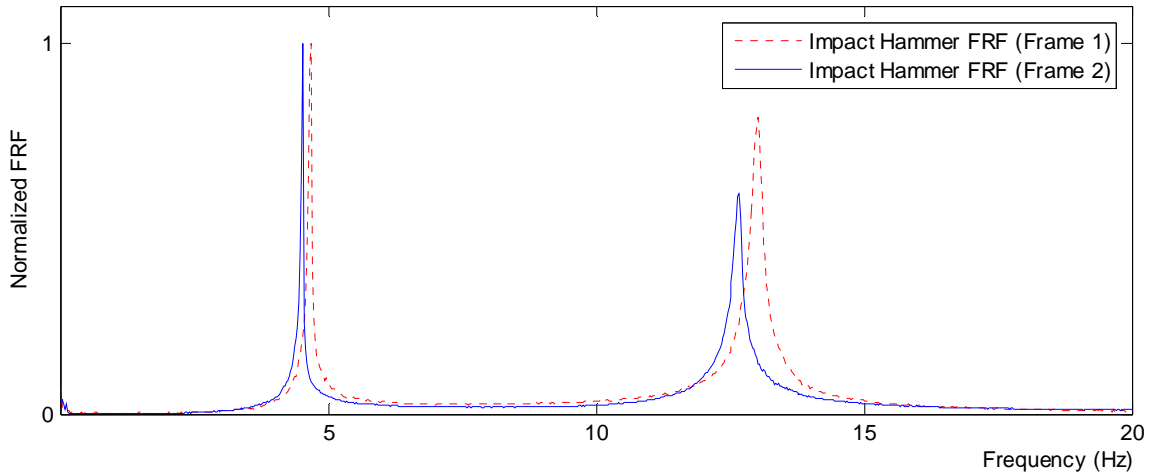


Figure 4. 37: Comparison of Impact Hammer FRF: Frame 1 vs. Frame 2

#### 4.4.3 LOW-AMPLITUDE SINUSOIDAL GROUND MOTION TESTING

Low-amplitude sinusoidal ground-motion testing was repeated on the experimental model with Frame 2 installed into the leaner frame. The same testing protocol, accelerometer measurement settings, and equipment used to test Frame 1 were used to test Frame 2. A comparison of the normalized ODS FRF and the FRF calculated from the impact hammer test is shown in Figure 4.38. First and second resonant peaks for the ODS FRF of Frame 2 occurred at 4.05 Hz and 11.5 Hz, respectively, which were 5.8% and 3.3% lower than those measured for Frame 1. The relative difference in shape of the FRF's for Frame 2, including the shift of resonant peaks to lower values for the ODS FRF from the impact hammer test, indicate that the FRF's were similar to those of Frame 1. A direct comparison of the ODS FRF's for both frames is shown in Figure 4.39.

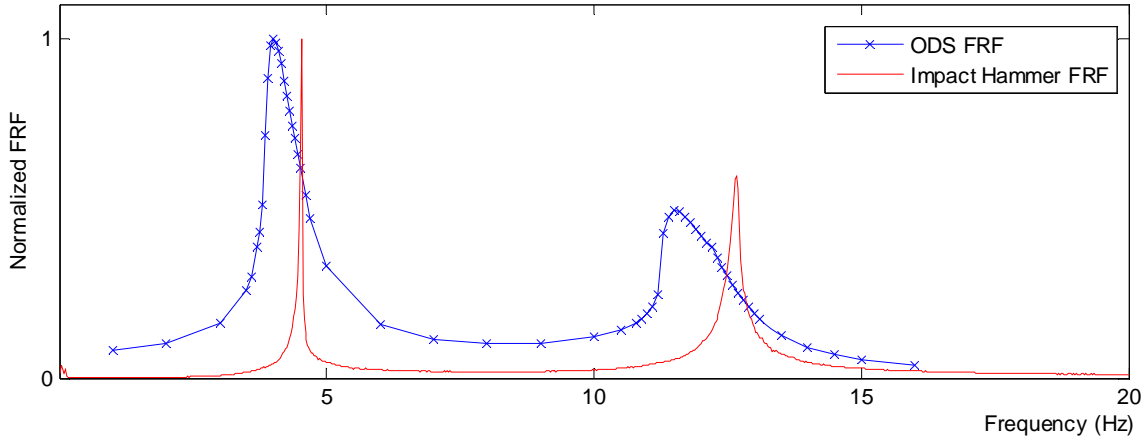


Figure 4.38: Comparison of Normalized FRF's (Frame 2)

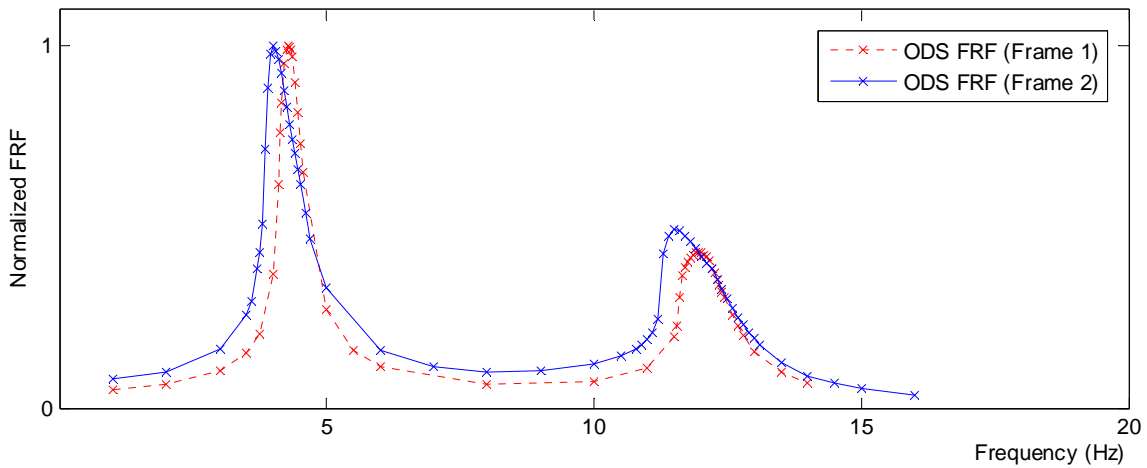


Figure 4.39: Comparison of ODS FRF: Frame 1 vs. Frame 2

After determining the resonant frequencies of vibration, the frame was shaken at each frequency until steady state was reached. At that point the ground motion input was stopped and the frame was allowed to decay freely. Frame 2 was shaken at the first resonant frequency. The normalized roof displacement was plotted (Figure 4.40), and the viscous damping model, described in subsection 4.3.4, was plotted over the roof displacement decay trace (Figure 4.41). Frame 2 was then shaken at the second resonant frequency. The normalized roof displacement was plotted (Figure 4.42), and the viscous damping model was plotted over the roof displacement decay trace (Figure 4.43). Damping was estimated to be approximately 3% of critical in the first mode and approximately 2.5% in the second mode. These values were 0.5% higher than those estimated for Frame 1.

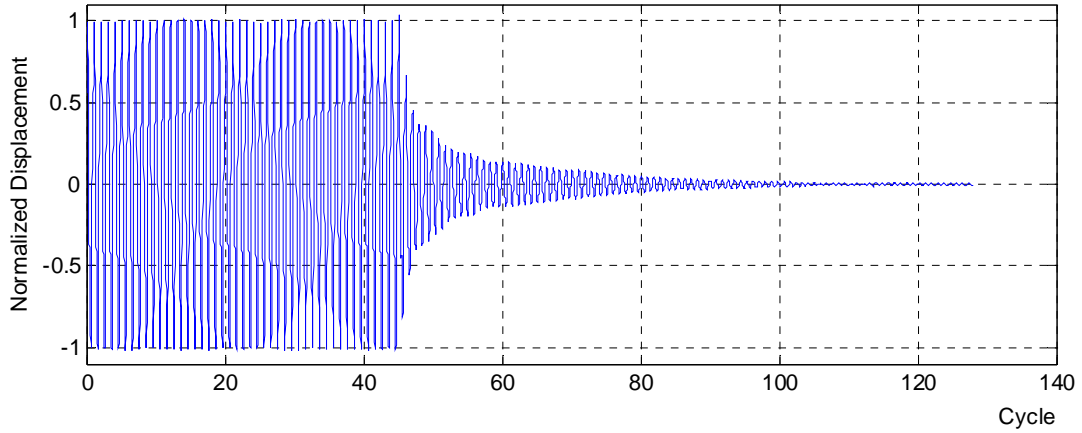


Figure 4. 40: Normalized Roof Displacement Decay (Frame 2, 4.05 Hz)

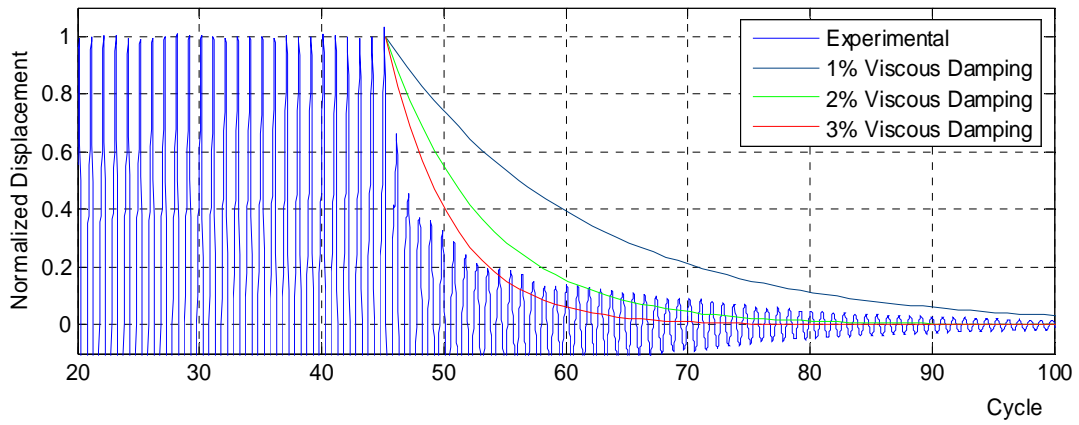


Figure 4. 41: Comparison of Roof Displacement Decay with Viscous Damping Model (Frame 2, 4.05 Hz)

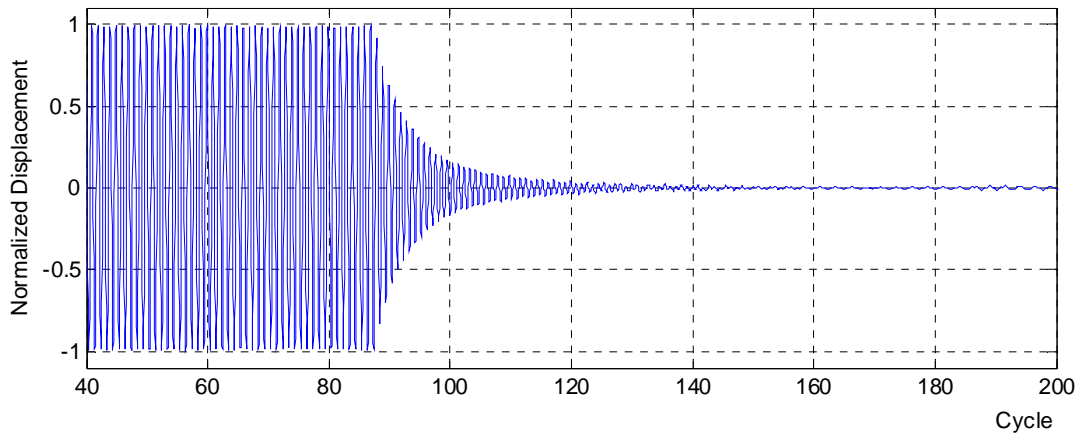


Figure 4. 42: Normalized Roof Displacement Decay (Frame 2, 11.5 Hz)

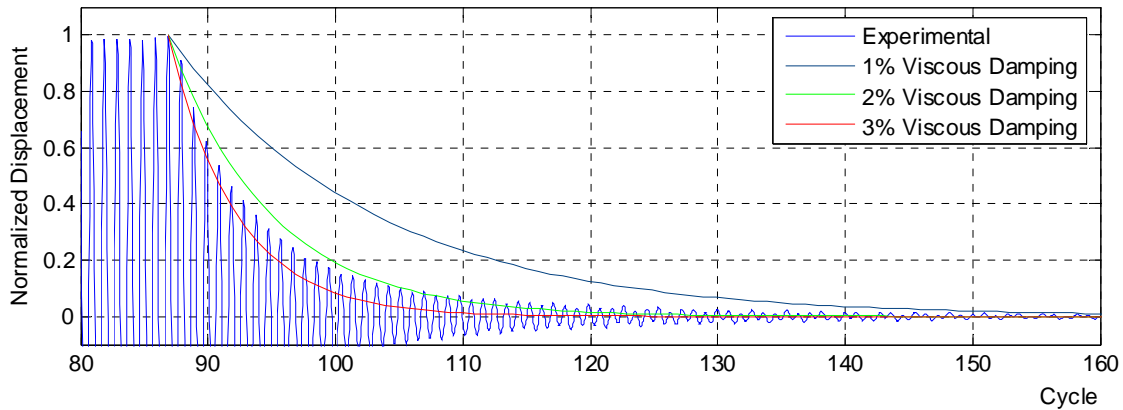


Figure 4. 43: Comparison of Roof Displacement Decay with Viscous Damping Model (Frame 2, 11.5 Hz)

#### 4.5 RESULTS

Frame 1 and Frame 2 were subjected to a series of non-destructive tests after being fit-up into the leaner frame on the shaking table, and prior to subjecting them to the Northridge ground-motion testing described in Chapter 5.

The first goal of these tests was to use the results to development an accurate analytical model in DRAIN for the purpose of predicting the behavior of the frames when subject to large ground motion excitations. Results of the tests were used to modify the DRAIN model, developed in Chapter 3. Specifically, panel joint stiffness, additional stiffness due to the leaner frame, and damping of the DRAIN model were modified to match Frame 1 test results. The resulting DRAIN model was shown to be effective in predicting floor displacements, roof displacements, and base shear of the experimental frame when excited with base shear at the first resonant frequency. Calibration of the DRAIN model using the results of stiffness and modal testing was limited to elastic behavior and modal damping. The effect of post-yield nonlinear characteristics of steel on the dynamic response of the frame was not experimentally quantifiable. Instead, nonlinear steel behavior was estimated in the DRAIN model based on well-documented characteristics of steel frames.

The second goal of stiffness and modal testing was to ensure that Frame 1 and Frame 2 were effectively the same. The basis of comparison for these frames was static stiffness, resonant frequencies calculated from impact hammer tests, and resonant frequencies determined through low-amplitude sinusoidal base input, and decay. Based on tests of Chapter 4, it was determined

that the frames were similar enough to test Frame 1 with ropes and Frame 2 without ropes and compare their results directly.